CHAPTER – 3

CHARACTERIZATION TECHNIQUES

3.1. CATALYST CHARACTERIZATION RESULTS

Prepared catalysts were characterized by various techniques such as low-temperature N_2 adsorption-desorption isotherms, XRD, XPS, SEM-EDS, FTIR and TEM. Here, the characterization section was categorized in terms of catalyst activity explained in prior section. The details of characterization results are mentioned below:

3.2. XRD results

The XRD studies were carried out to identify the phases present in the catalyst samples by collecting intensity data over a 2θ = 20-80°. The XRD patterns of the $MnCo_2O_4$ catalysts are shown in Figure 3.1, which confirmed the formation of spinel structure in all prepared catalysts. The common miller indices of the catalysts ($MnCo_2O_4$) corresponding to the obtained peaks at 30.9, 36.3, 44.2, and 64.7 are (2 2 0), (3 1 1), (4 0 0), and (4 4 0), respectively (PDF#65-6920; 23-1390; 23-1237) [160].

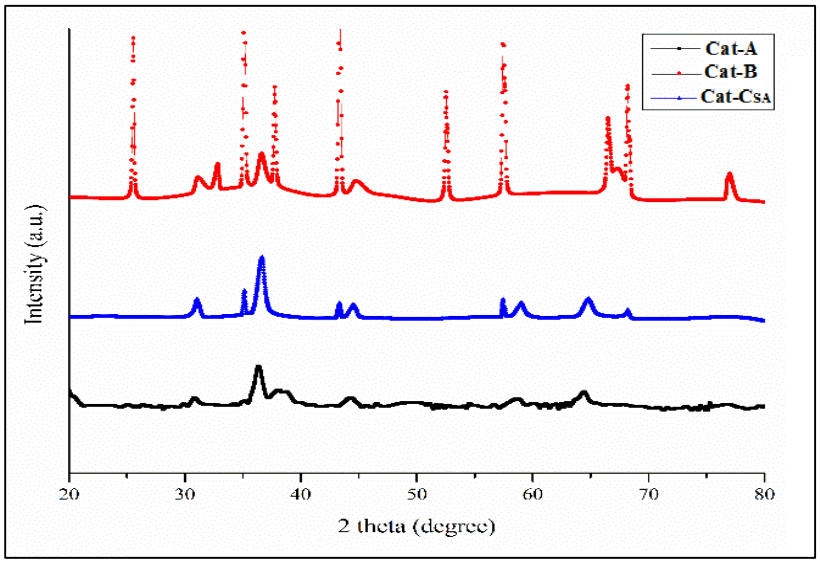

Figure 3.1. XRD of Cat-A, Cat-B and Cat-C_{SA}

It is very clearly observed from the figure that XRD pattern of the cobaltites is almost similar. Only the peak related to spinel was observed; no extra peak was detected in the figure, consequently signifying the purity of the sample. The low intensity of peaks for Cat-C_{SA} represented its highly quasi-crystalline nature with the smallest crystallite size among the others. The crystallite sizes of the catalysts were calculated using Debye – Scherrer equation as stated in Table 3.1.

Table 3.1. Crystallite size of Cat-A, Cat-B and Cat-C_{SA}.

Catalysts	Crystallite size (nm)
Cat-A	8.01
Cat-B	8.57
Cat-C_{SA}	8.48

The XRD studies were carried out to identify the planes present in the catalyst samples by collecting intensity data over a 2θ = 20-80°. XRD patterns of $MnCo_2O_4$ catalysts synthesized by DCP method based on their calcination strategies are displayed in Figure 3.2. The characteristic reflections showed diffraction peaks at 2θ = 36.71°, 64.93°, 59.00°, 31.17°, 44.48° and 38.33° could be primarily attributed to a spinel structure JCPDS card no. 32-0297 correspond to the (311), (440), (511), (220), (400) and (222) planes of $MnCo_2O_4$, respectively. The sharp peaks in Cat-C_{RC} indicate crystalline nature of average size of 12.02 nm of $MnCo_2O_4$ and justified by [JCPDS no.32-0297]. The peaks indicated the presence of the spinel $MnCo_2O_4$ of nano-size crystallites [161]. In the XRD pattern less intense single peak at 77.0° was found in Cat-C_{SA} as secondary phase ascribed to (402) plane of $Mn_{0.98}O_2$ corresponds to JCPDS card

no. 81-1947. The powder XRD patterns of the ordered mesostructured and crystalline nature of $MnCo_2O_4$ were confirmed.

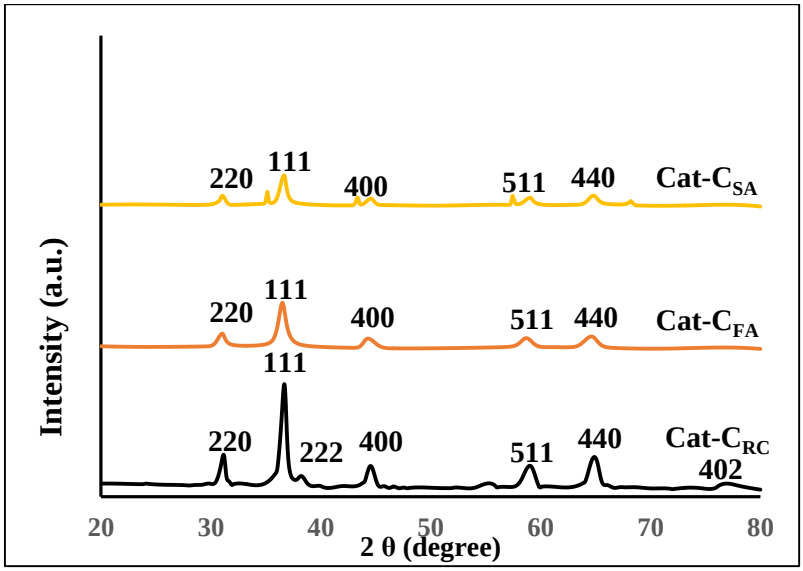

Figure 3.2. X-ray patterns of different $MnCo_2O_4$ catalysts based on their calcination strategy

XRD studies were carried out based on different metal cobaltites catalyst samples. The transition metal cobaltites and crystalline nature of $CuCo_2O_4$, $MnCo_2O_4$, $NiCo_2O_4$ were confirmed by XRD. The XRD patterns of all three spinel catalysts synthesized by nano-casting methods are displayed in Figure 3.3.

The characteristics reflections of $CuCo_2O_4$ showed diffraction peaks at 2θ= 31.07°, 35.54°, 36.63°, 38.66°, 44.57°, 59.01° and 64.84° could be primarily attributed to a spinel structure referred from JCPDS card no.# 37-0878, which corresponds to the (200), (311), (311), (222), (400), (333) and (440) phase structure of $Cu_{0.92}Co_{2.08}O_4$, respectively. From the Scherer's formula, average crystallites size of $CuCo_2O_4$ is 34.78 nm.

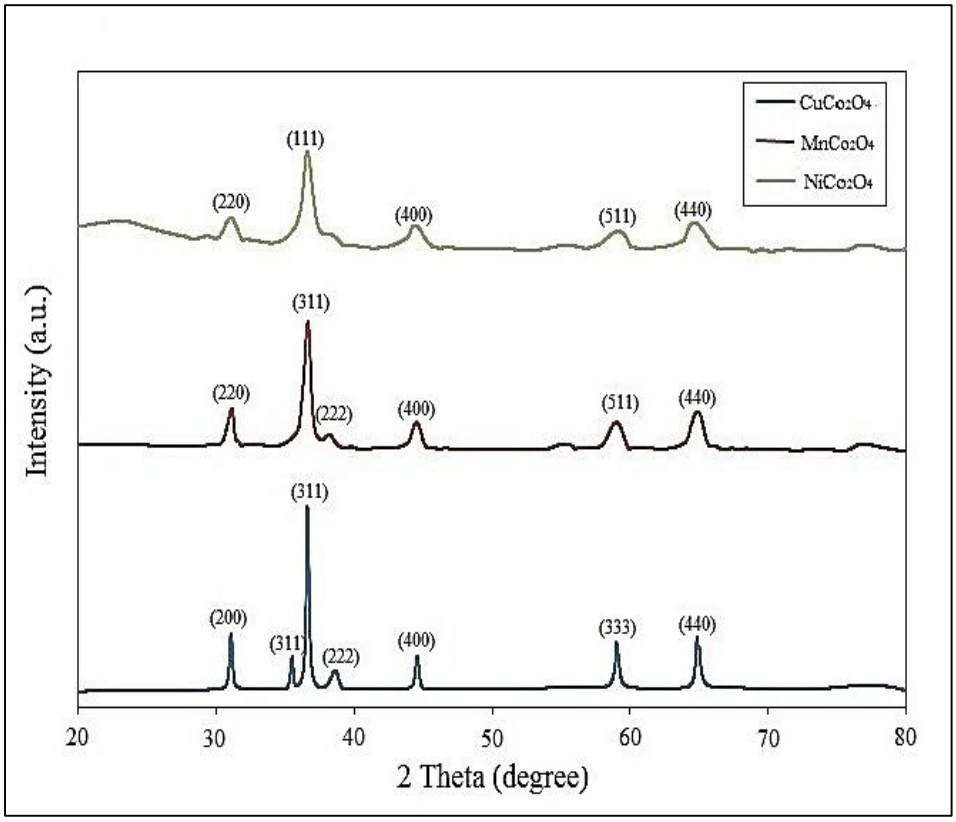

Figure 3.3. X-ray diffractogram of $CuCo_2O_4$, $MnCo_2O_4$ and $NiCo_2O_4$ catalysts

Table 3.2. Crystallite size of the prepared catalyst samples

Catalyst	Crystallite size (nm)
$NiCo_2O_4$	33.54
$MnCo_2O_4$	12.02
$CuCo_2O_4$	34.78

The characteristics reflections showed diffraction peaks at 2θ= 36.71°, 64.93°, 59.00°, 31.166°, 44.48° and 38.33° could be primarily attributed to a spinel structure JCPDS card no. # 32-0297 corresponds to the (311), (440), (511), (220), (400) and (222) phase structure of $MnCo_2O_4$ [22, 23]. In the XRD pattern less intense single peak at 77.0° was found as secondary phase ascribed

to (402) phase structure of $Mn_{0.98}O_2$ corresponds to JCPDS card no. # 81-1947. The high intensity sharp peak in $MnCo_2O_4$ indicate crystalline nature and average crystallites size of 12.02 nm is calculated by Scherer's formula, and justified by [JCPDS card no. #32-0297].

The characteristics reflections showed diffraction peaks at 2θ= 36.93°, 64.74°, 58.83°, 31.09°, 44.72° and other two 23.4°, 54.83° could be primarily attributed to a spinel structure JCPDS card no. # 10-0188, 40-1191, 73-1702, 02-1074, 89-7728 corresponds to the (111), (440), (511), (220), (400) and (110), (310) phase structure of $NiCo_2O_4$ average crystallites size from Scherer's formula is 33.54 nm. The intensity of the diffraction peaks of the different cobaltite catalysts increases in the following order: $NiCo_2O_4$ <$CuCo_2$ O_4 < $MnCo_2O_4$.

Effect of metal cobaltites loading on γ-Al_2O_3 were shown in the XRD of the RC calcined catalysts are shown in Figure 3.4. The diffraction pattern with standard peaks at 2θ values of 37.26°, 43.16^o, 62.7^o, and 75.2^o assigned to diffracting planes (111), (200), (220), and (311) respectively, was fcc type Mn_2O_3 (JCPDS# 78–0423). Kalam et al. had shown almost similar XRD pattern of nano-size CoO [43]. Therefore, it was confirmed that CoO was formed by RC route. The XRD pattern of Co_{RC} confirmed the formation of cubic phase Co_3O_4 spinel with 2h values 30.06, 36.8, and 59.5 degrees assigned to (220), (111), and (511) diffracting planes respectively as presented in the figure (JCPDS# 26–4356 or 76–1802). Babu et al. reported the almost similar pattern of Co_3O_4. So, it was assured that the normal spinel of Co_3O_4 was formed by RC route [44].

The structure of γ-Al_2O_3 is traditionally considered as a cubic defect spinel type in which the oxygen atoms are arranged in a cubic close packing and Al atoms occupy the octahedral and tetrahedral sites. Gamma alumina phase was confirmed with the intensive and sharp diffraction

peaks at 37.53° (311), 45.67° (400), 60.54° (511) and 66.60° (440) could be primarily attributed to a cubic γ-Al_2O_3 structure (PDF-50-0741 JCPDS file).

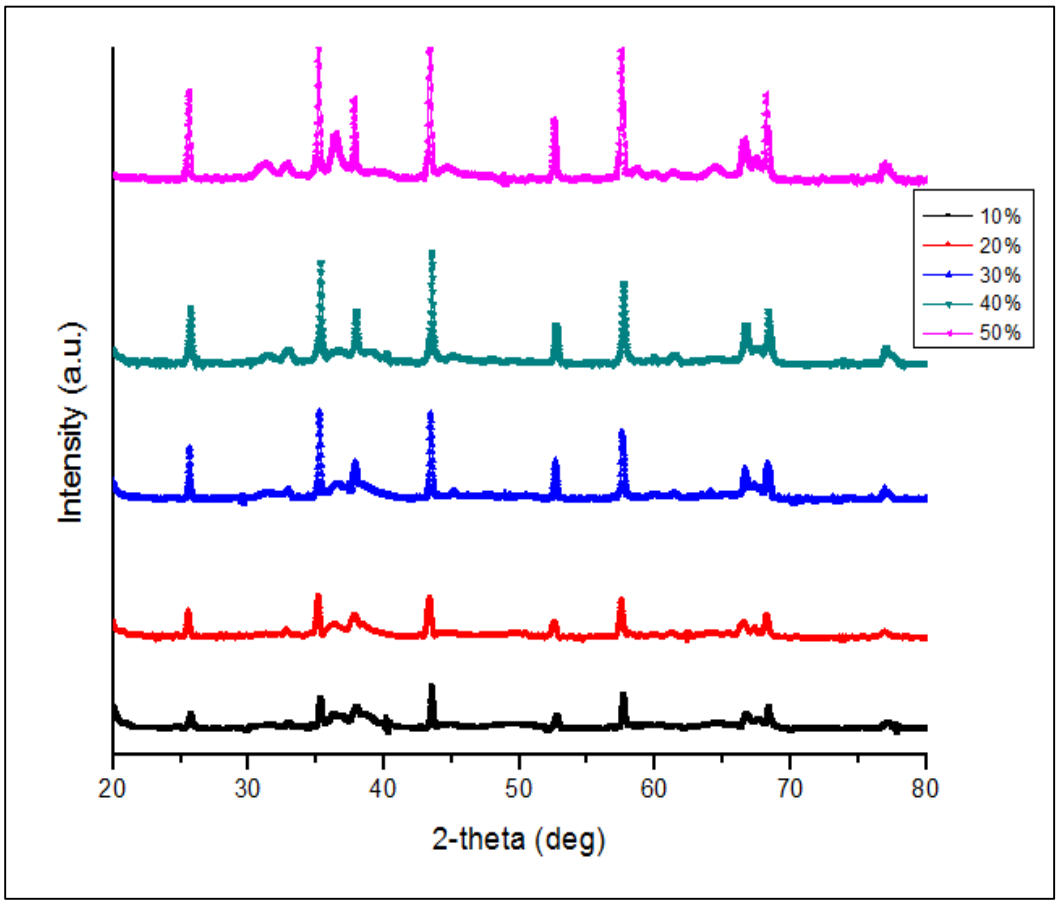

Figure 3.4 XRD pattern of $MnCo_2O_4$/γ-Al_2O_3 catalyst with different loading

The XRD pattern of different metal cobaltite loading was also illustrated in Figure 3.4. The diffraction peak at 2theta 31.40°, 36.71°, 38.44°, 44.81°, 55.7°, 59.3°, and 65.01° are indexed as crystal planes of (220), (311), (222), (400), (422), (511), and (440) respectively of $MnCo_2O_4$ (JCPDS# 20–0781). The XRD spectra confirmed the $MnCo_2O_4$ spinel structure of the catalyst which was also in good agreement with the literature [18, 45]. The parameter values were close to the literature values.

the catalyst which was also in good agreement with the literature [18, 45]. The parameter values were close to the literature values. The crystallite size of 30% $MnCo_2O_4/\gamma\text{-}Al_2O_3$ was 8.061Å greater that of 10% and 20% loading but smaller than 40% and 50% loading. This is because 30% is the optimum Mn into Co_3O_4 spinel structure.

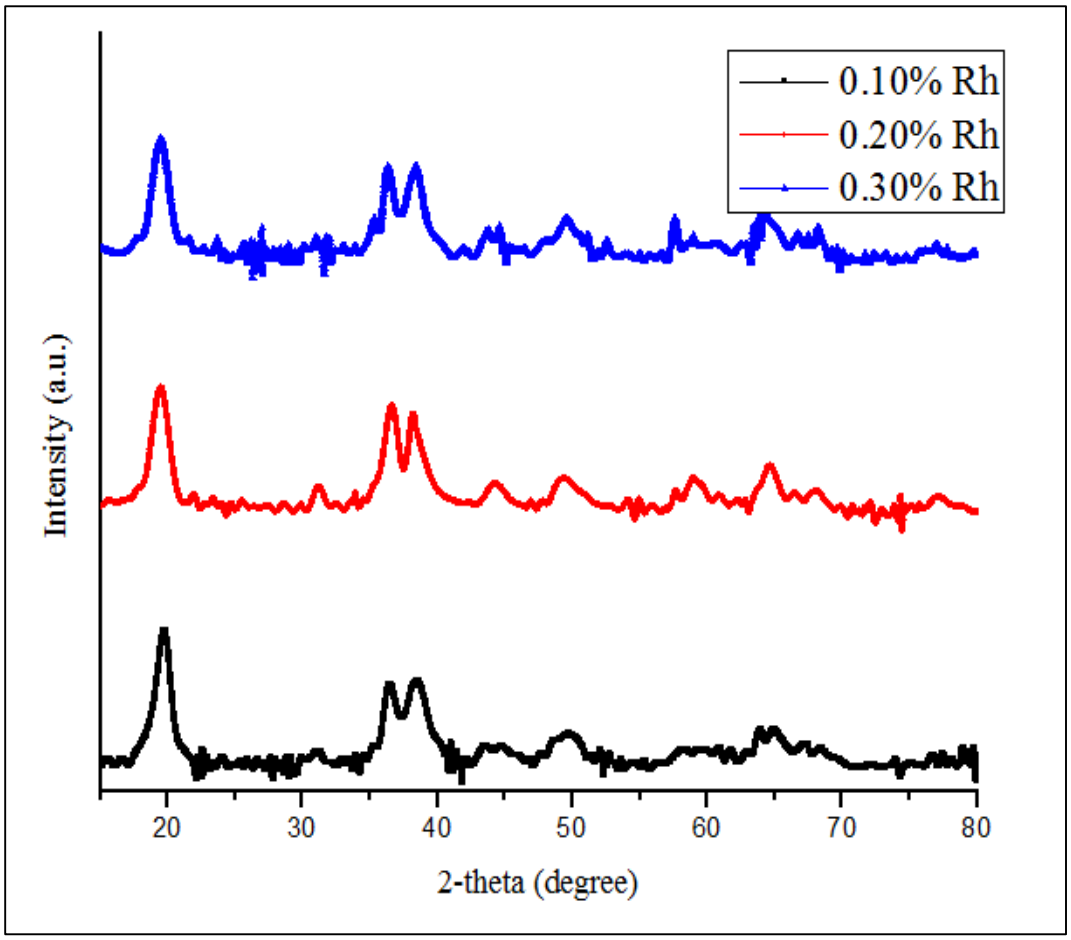

Figure 3.5. XRD pattern of Rh doped $MnCo_2O_4/\gamma\text{-}Al_2O_3$ catalyst.

The phase and purity of the catalysts were characterized by XRD and the patterns are shown in Figure 3.5 for promoter (Rh) doping. The common peaks (220), (311), (400), (511), (400) are indexed to a $MnCo_2O_4$ face centered cubic (fcc) crystal structure [JCPDS: 20-0781]. Distinctive lines of $MnCo_2O_4$ spinel in XRD patterns were observed in all catalysts. The

presence of dopants (Rh) was absent in the spectra, which indicated that the dopants were highly dispersed on the $MnCo_2O_4$ sample surface or in microcrystalline state that make it a stronger spinel phase for reaction. An additional peak was observed at 25.70 in Cat-K which might correspond the presence of Rh in the catalyst.

The XRD results might be described on the basis of an interaction between dopants and the spinel. The good dispersion of Rh in $MnCo_2O_4$ was giving an intimate contact which leads to a stronger tendency to stabilize the spinel phase for an improved active phase for SCR of NO. The doping of Rh did not cause an important change on the crystallinity of the catalysts. Thus, the doped catalysts were maintained in the cubic structure.

The sharp peaks in V-W-Ti catalyst indicate relatively crystalline nature of the catalyst and formation of average crystallites size of 120.2 Å. It is quite apparent that crystallites form by RC of the catalyst precursors of Cat-K exhibited smallest size (7.97 nm) in comparison to V-W-Ti (11.2 nm) is incorporated in Figure 3.6.

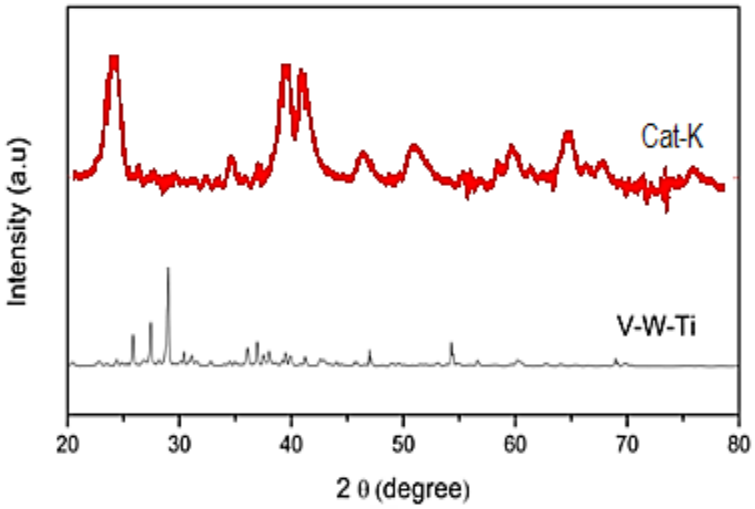

Figure 3.6. X-ray diffraction patterns of Cat-K and V-W-Ti.

3.2. XPS results

The elemental composition and surface valence state of the catalysts were characterized by XPS analysis. The XPS spectra of the cobaltites in the Mn2p, Co2p, and O1s regions. Using Gaussian fitting methods, it was clearly observed that the Co2p spectra of all cobaltites catalyst consist of two main peaks fitted at the range of binding energies of 780.12 – 781.6 eV are recognized to Co^{2+}, while the peaks at 777.75 and 783.39 eV are ascribed to Co^{3+} [34]. The ratio of Co^{2+}/Co^{3+} for all cobaltites is Cat-C_{SA} < Cat-B < Cat-A, although it can be suggested that high Co^{2+}/Co^{3+} is preferable for the reduction reaction [38]. For Cat-C_{SA}, the two oxidation state were noticed in Mn2p spectra and attributed to Mn^{2+} and Mn^{3+} ions. The peaks fitted at 641.5 and 653.4 eV were attributed to Mn^{2+}, and peaks at 643.5 and 654.5 eV were recognized to the existence of Mn^{3+} [36,41].

The two main oxygen contributions are shown in O1s spectra and denoted as O ads (surface oxygen) and O lat (lattice oxygen). Remarkably, the O_{ads} constituent with binding energy 529.2 – 530 eV is reliable with metal – oxygen bonds, whereas the O_{lat} element with binding energy 531.3 –532.2 eV relates to a large no defect sites with low coordination oxygen. From the figure, it can be seen that Cat-C has well-resolved peak of lattice oxygen, which is comparable with Cat-A. Thus, it is well known that the defects/dislocations are desirable to enhance the active sites for the oxidation reaction. The high ratio of O_{ads} /(O_{ads} + O_{lat}) is desirable for highly active catalysts also. This ratio for all catalysts is as follows: Cat-C_{SA} > Cat-B > Cat-A.

XPS results analysis investigated for comparative calcination strategies for the surface valence state and concentration of Cat-C_{RC}. Figure 3.7. (a-c) displays the XPS spectra in the Co-2p, Mn-2p and O-1s regions. The XPS spectra in the Mn-2p region are presented in Figure 3.7.(a). The observed binding energies 644.1 eV, and 658.4 eV are associated with the presence of Mn^{2+} and Mn^{3+} respectively in Cat-C_{RC} sample [40].

In Figure 3.7. (b) shows the two major peak of Co-$2p^{3/2}$ level was centered at 783.1 and 798.4 eV attributed to Co-$2p^{3/2}$ and Co-$2p^{1/2}$ configurations. Although, it can be proposed that highest Co^{3+}/Co^{2+} are preferable for the reduction of NO [41]. The binding energies of O-1s are displayed in Figure 3.7. (c). Generally, there are two different types of oxygen in the catalysts with binding energy 532.2 eV and 534.1 eV, which could be predictable as chemisorbed oxygen and lattice oxygen, respectively. The presence of chemisorbed oxygen is small as compared to lattice oxygen in Cat-C_{RC}.

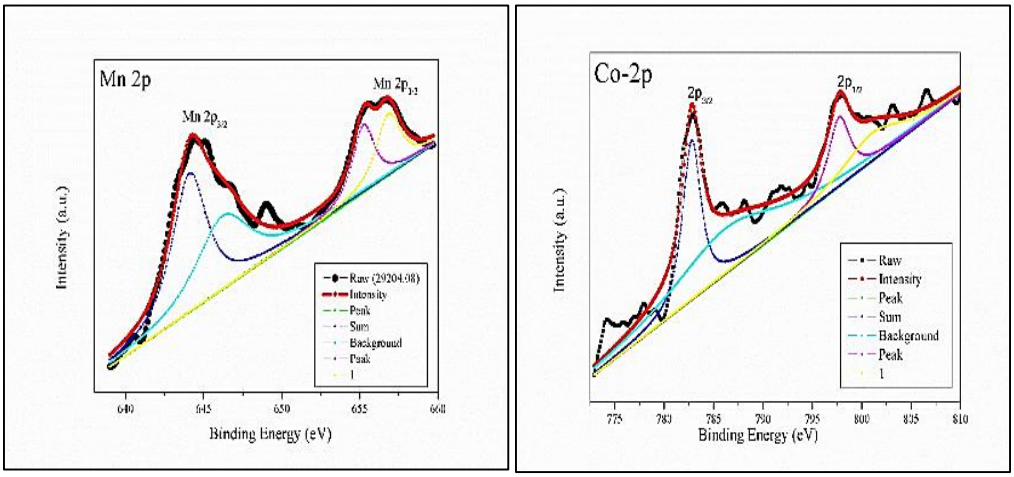

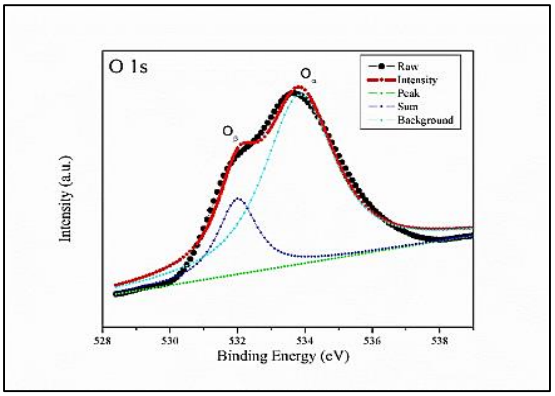

Figure 3.7. XPS spectra of Cat-C_{RC} (a) Mn-2p; (b) Co-2p; and (c) O-1s.

Analysis of XPS results observed the surface valence state and concentration of $MnCo_2O_4$. XPS spectra in the Mn-2p, Co-2pand O-1s regions presented the observed binding energies 644.1 eV, and 658.4 eV are associated with the presence of Mn^{2+} and Mn^{3+} respectively in $MnCo_2O_4$ sample for different metal cobaltites is hown in Figure 3.8.

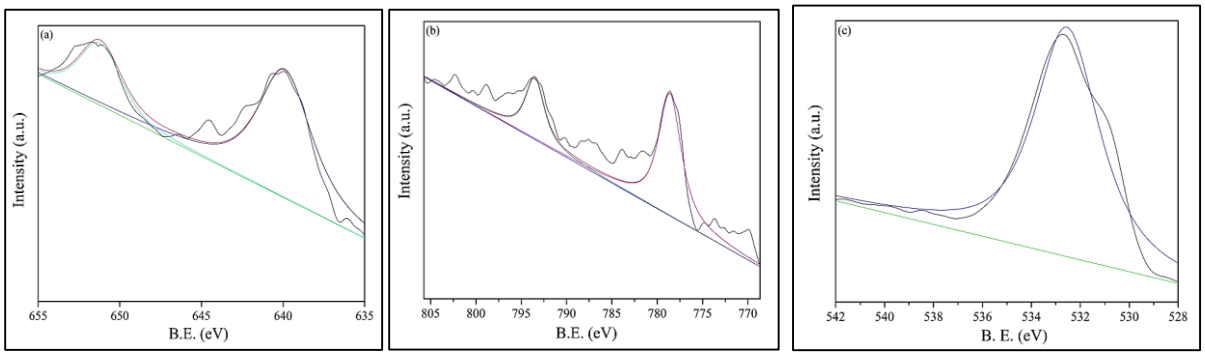

Figure 3.8. XPS peak fitting of Cat-I (a) Mn-2p, (b) Co-2p and (c) O-1s for $MnCo_2O_4$.

The two major peak of the Co-$2p^{3/2}$ level was cantered at 783.4 and 798.3 eV attributed to Co-$2p_{3/2}$ and Co-$2p_{1/2}$ configurations as shown in Figure 3.8. Although, it can be anticipated that highest Co^{3+}/Co^{2+} are preferable for the reduction of NO. Generally, the oxygen has binding energy 534.1 eV, which could be predictable as lattice oxygen, respectively.

In order to examine the chemical bonding states and compositions of the surface elements of the catalysts, the samples were studied by XPS, and results are shown in Figure 3.9. In the spectrum of Co2p, two kinds of Co species containing Co^{2+} and Co^{3+} were observed in Cat F-Cat-I. The peaks fitted at 780.19 eV and 781.4 eV were indexed to Co^{3+} and Co^{2+}, respectively. A small peak at 777.01 was subjected to a Co^{2+} shakeup satellite peak of $MnCo_2O_4$. In doped catalysts, the peaks of Co^{3+} and Co^{2+} were shifted to low binding energies. Thus, the chemical shift is reasonable to consider that there was a direct interaction of the internal donor with the dopants in $MnCo_2O_4$. The ratio of Co^{2+}/Co^{3+} is the lowest in Cat-H which is preferable for reduction reaction.

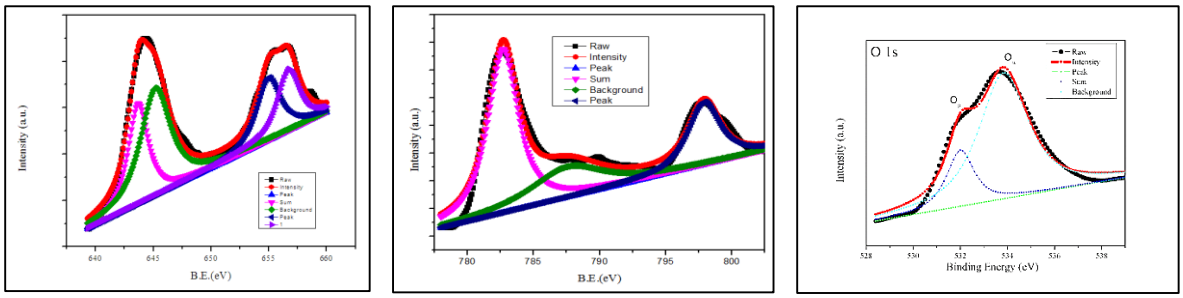

Figure 3.9. XPS peak fitting of Cat-K (a) Mn-2p, (b) Co-2p and (c) O-1s.

The Mn2p spectra of all catalysts given in Figure 3.9 were fitted considering two spin orbit doublets as characterstics of Mn^{2+} and Mn^{3+} and a shakeup setallite. The fitting peak at the binding energy of 659.5 eV was indexed to Mn^{2+}, while the fitting peaks at 644.1 eV and 658.5 eV were attributed to Mn^{3+}, respectively. The peaks of Mn^{2+} and Mn^{3+} were also present in all the catalysts. Alumina has been widely studied as support for catalysts loading due to its stability with SCR of NO.

The same two peaks (644.1 eV and 658.5 eV) for Mn at $3d_{5/2}$ and 340.3 eV for $3d_{3/2}$, respectively. The binding energy of Rh was near to the value of 308.9 eV, which is a

characteristic peak of Rh_2O_3, indicating the presence of Rh in both Cat-J, cat-K and Cat-L catalyst. The ratio Rh_2O_3/Rh(0) was calculating using the XPS peak area was 4.5 and 5.7 in Cat-K, respectively. Rh_2O_3 is the main active component and especially favourable for NO reduction. The NO-SCR used the oxygen from the Rh_2O_3 component and then the reduced metal Rh is re-oxidized during the oxygen mobility of the catalyst. These results of the Mn, Co, Al and Rh spectra of Cat K exhibited that the surface of a spinel contained Mn^{2+}, Mn^{3+}, Co^{2+} and Co^{3+}, while doped catalysts also showed Rh^{3+}, except the common element. The O1s spectra of the doped and undoped $MnCo_2O_4$ catalyst remained the same. It was reported in the literature that a peak at 529 eV (O_α) represents the nucleophilic oxygen (O_2) and a peak at 532 eV (O_β) represents the electrophilic oxygen (O). The nucleophilic oxygen (O_2) is responsible for the reduction, while the electrophilic oxygen (O) is related to the total oxidation of hydrocarbon. It can be seen from the figure that both oxygens peaks are present in all catalysts. The content order of the O_β /(O_β + O_α) ratio was shown as follows: Cat-K > Cat-J > Cat-L.

3.3. SEM-EDS results

The SEM study was used to investigate the morphology of the catalysts. The SEM images of the prepared catalysts are shown in Figure 3.10. From the figure, it can be seen that cobaltites exhibited noticeable dissimilarities in micrographs. Cat-A seems like to round shape, whereas quasi-spherical particles of different sizes were observed in Cat-B, and Cat-C_{SA}. The large lump particles were found in Cat-B. The particle sizes of the catalysts were calculated using Image J software. The particles of Cat-C_{SA} are smaller as compare with other catalysts. The differences in the particle size (Dp) and the crystal size (Dc) vary from 54.35 to 96.89 nm for different catalysts. The particle size in ascending order in the catalysts is as follows: Cat-C_{SA} < Cat-B < Cat-A. The number of crystallites per particle (Dp/Dc) in all the catalysts

is around 7 except Cat-A for which it is round about 8. To check the purity of the catalysts, the elemental composition was determined by EDX analysis.

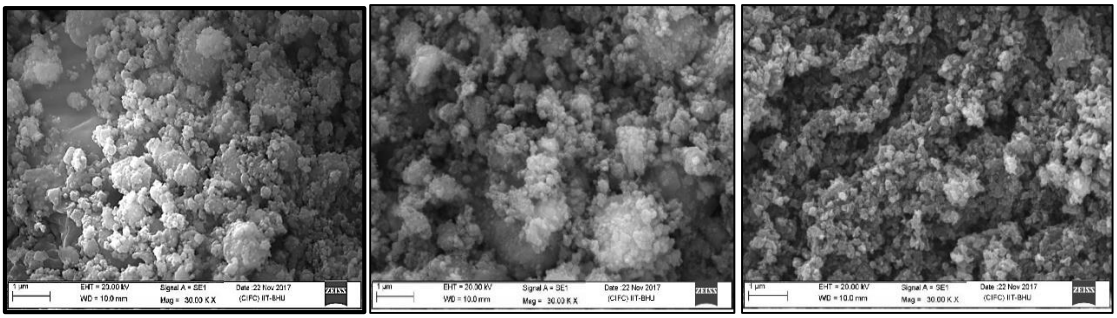

Figure 3.10. SEM micrographs of (a) Cat-A; (b) Cat-B; and (c) Cat-C_{SA}.

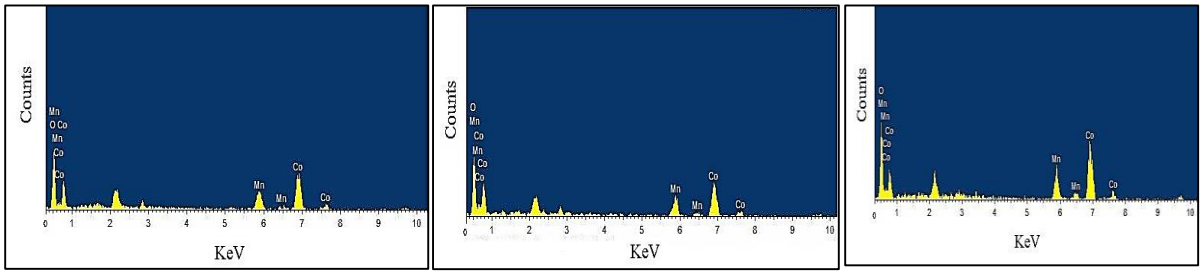

Figure 3.11. EDX spectrum and elemental micrographs of (a) Cat-A; (b) Cat-B; and (c) Cat-C_{SA}.

Figure 3.10 shows the EDX spectrum of manganese cobaltites, which confirmed the presence of Mn, Co, O) elements. Their atomic percentages are mentioned in Table 3.3. It is clearly indicated that the precursors completely precipitated during synthesis in CP and DCP. The stoichiometric ratio is almost the same in all the catalysts as used in the preparation. The low atomic percent (%) of oxygen in all catalysts confirmed the presence of oxygen deficiency in the catalysts that is created by NC.

Table 3.3. Weight % and atomic % (EDX elemental data) for Cat-A, Cat-B and Cat-C_{SA}

	Cat-A		Cat-B		Cat-C_{SA}	
Element	Weight%	Atomic%	Weight%	Atomic%	Weight%	Atomic%
O K	20.34	48.03	27.85	58.12	32.60	58.62
Mn K	19.44	13.37	24.26	14.75	17.42	13.90
Co K	60.22	38.60	47.89	27.13	49.98	26.48
Total	100.00		100.00		100.00	

SEM micrographs of the catalysts were recorded to examine the morphology and structure of the $MnCo_2O_4$ materials. Figure 3.12 shows the electron micrographs of Cat-C_{SA}, Cat-C_{FA} and Cat-C_{RC}. All the catalysts particles were of spherical morphology and more or less uniform size distribution. But the size of the particles was larger in case of Cat-S than that of Cat-C_{RC}. Thus, the DCP technique of catalyst preparation followed by reactive calcination considerably affects the particle size and morphology of the respective catalysts.

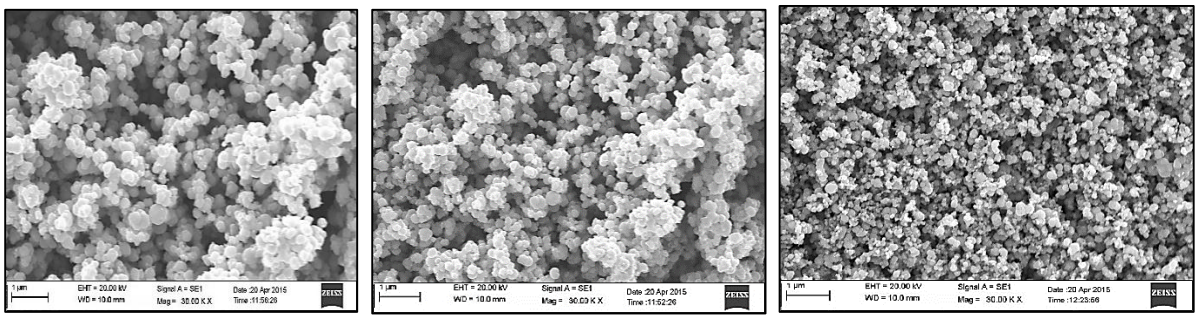

Figure 3.12. SEM micrographs of (a) Cat-C_{SA}; (b) Cat-C_{FA}; and (c) Cat-C_{RC}.

The SEM micrographs in Figure 3.12 (a-c) show that catalysts were composed of the mono-disperse homogeneous spherical nanoparticles. The micrographs of these three catalysts show clearly large differences in the microstructure and morphology of these spinel catalysts. The granular particles calculated by "Image J software" range between 0.66 and 9.69 nm. The particles shown in SEM micrograph comprised grains of course, fine and finest sizes. The same result complied from the crystallite size calculated based on XRD data as well. Particles of Cat-C_{RC} are less agglomerated, porous and uniform as compared to other catalyst samples. Sizes of crystallites as well as particles of Cat-C_{SA} are relatively very large and agglomerated than Cat-C_{RC} and Cat-C_{FA}. Thus, the DCP technique followed reactive calcination in the

present study considerably affect the porosity, particle size and morphology of the respective catalysts. As displayed in Figure 3c SEM image, the resultant $MnCo_2O_4$ products are uniform and well-dispersed microspheres. The high-magnification SEM photographs demonstrate firmly nanosized interconnected microspheres. High quality uniform $MnCo_2O_4$ microspheres could be improved by reactive calcinations technique.

The elemental composition of the $MnCo_2O_4$ microspheres was first examined by EDX measurements. EDX results from different regions of micrographs depicts that all the samples were pure due to presence of Co, Mn and O peaks and no other element present in the spectra as shown in Figure 8.

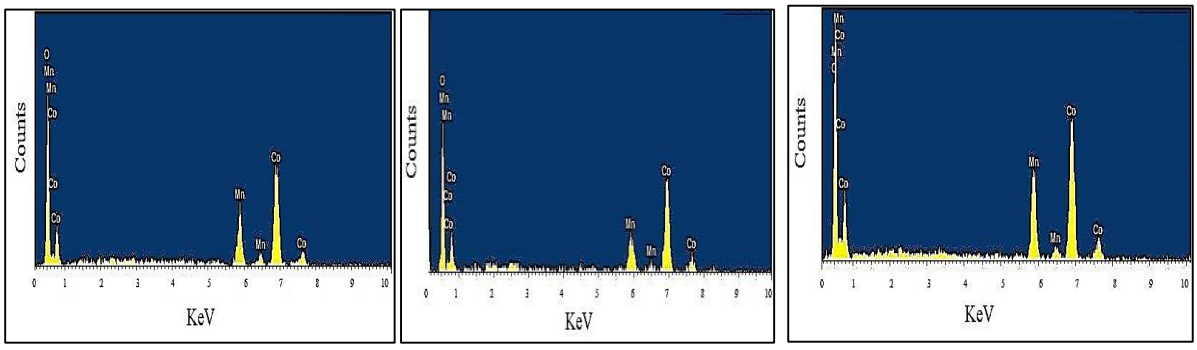

Figure 3.13. EDX spectrum and elemental micrographs of (a) Cat-C_{SA}; (b) Cat-C_{FA}; and (c) Cat-C_{RC}.

EDX spectrum of the $MnCo_2O_4$ sample only gives signal peaks of Mn, Co, and O elements with a Co/Mn ratio of about 2:1. The EDX data results from the catalyst surface with relative weight and atomic compositions in their respective catalyst samples are tabulated in Table 3.4. Presence of respective pure oxides phase in the sample complies with XRD and FTIR data.

Table 3.4. Weight % and atomic % (EDX elemental data) for Cat-C_{SA}, Cat-C_{FA} and Cat-C_{RC}.

	Cat- C_{SA}		Cat- C_{FA}		Cat-C_{RC}	
Element	Weight%	Atomic%	Weight%	Atomic%	Weight%	Atomic%
O K	20.34	48.03	27.85	58.12	32.60	58.62
Mn K	19.44	13.37	24.26	14.75	17.42	13.90

Co K	60.22	38.60	47.89	27.13	49.98	26.48
Total	100.00		100.00		100.00	

It is clear from the table that atomic and weight percentage of Co is higher than the Mn in all three catalysts. However, the atomic composition of Co and Mn in Cat-R is much closer to stoichiometric ratio of preparation method rather than Cat-C_{SA} and Cat-C_{FA} and the atomic composition of oxygen is less in Cat-C_{RC}. It means there is oxygen deficiency in Cat-C_{RC} creating high density of active sites consequently, enhancing the activity of the catalyst.

Elemental mapping analysis and corresponding EDX-mapping images of the $MnCo_2O_4$ spheres clearly elucidate homogeneous distribution of Mn, Co, and O elements further confirm the formation of pure $MnCo_2O_4$ materials and the best distribution in Cat-R as depicted from other characterization techniques.

Here, SEM analysis was done to identify the morphology of the different cobaltite catalysts. The electron micrographs of $CuCo_2O_4$, $MnCo_2O_4$ and $NiCo_2O_4$ in Figure 3.14 (a-c). All the catalyst having particles of spherical morphology and more or less uniform size distribution. But the size of the particles larger with more cluster in the case of $CuCo_2O_4$ and $NiCo_2O_4$ while smaller particle size in $MnCo_2O_4$. Thus, the nano-casting technique followed for $MnCo_2O_4$ in the present study considerably affects the particle size and morphology of the respective catalysts.

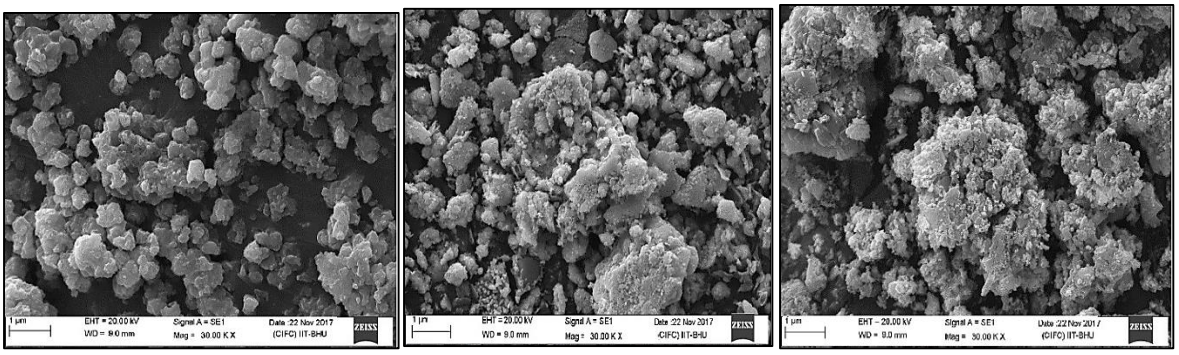

Figure 3.14. SEM micrographs of (a) $CuCo_2O_4$, (b) $MnCo_2O_4$ and (c) $NiCo_2O_4$.

SEM measurements were conducted to examine the morphology and structure of the $MnCo_2O_4$ materials. The granular particles calculated by "Image J software" range between 5.96 and 10.89 nm. As displayed in Figure 3.14. (b) SEM image, the resultant $MnCo_2O_4$ products are uniform and well-dispersed microspheres. Dispersion and surface area of catalyst promote catalyst activity as reported previously [124].

The elemental composition of the $CuCo_2O_4$ $MnCo_2O_4$ and $NiCo_2O_4$ microspheres was examined by Energy Dispersive X-ray (EDX) measurements. Energy dispersive X-ray (EDX) results from different regions of micrographs shown in Figure 3.15 depicts that all the samples were pure due to the presence of Co, Cu, Mn, Ni and O peaks and no other element observed in the spectra.

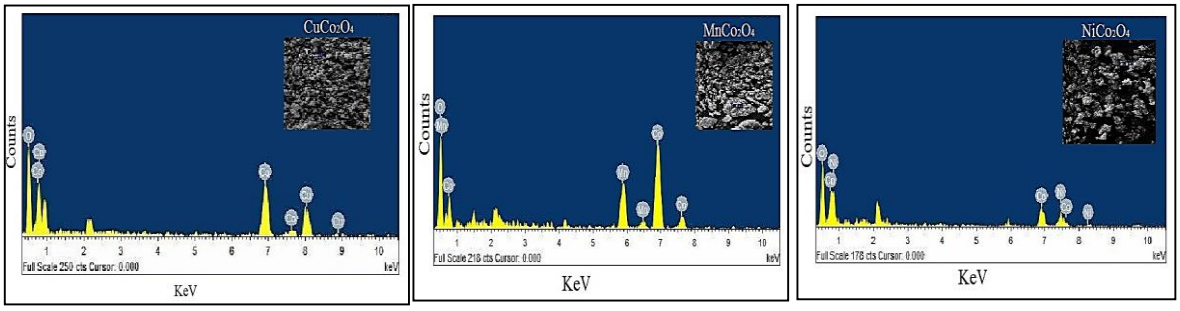

Figure 3.15. EDX spectrum and elemental micrographs of (a) $CuCo_2O_4$ (b) $MnCo_2O_4$ and (c) $NiCo_2O_4$

Table 3.5. Weight % and atomic % (EDX elemental data) for $CuCo_2O_4$, $MnCo_2O_4$ and $NiCo_2O_4$

	$CuCo_2O_4$		**$MnCo_2O_4$**		**$NiCo_2O_4$**	
Element	**Weight%**	**Atomic%**	**Weight%**	**Atomic%**	**Weight%**	**Atomic%**
O K	29.77	61.67	28.32	58.86	46.15	75.92
Co K	40.94	23.05	54.65	30.81	33.44	14.94
Cu/ Mn/ Ni K	29.29	15.28	17.03	10.33	20.41	9.14
Total	100.00		100.00		100.00	

EDX spectrum of the $MnCo_2O_4$ sample only gives signal peaks of Mn, Co, and O elements with a Co/Mn ratio of around 2:1. The EDX data results of relative weight and atomic compositions in their respective catalyst samples are tabulated in Table 3.5.

Presence of respective pure oxides phase in the sample complies with XRD results. It is clear from the table that atomic and the weight percentage of Co is higher than the Cu, Mn and Ni in all three catalysts. However, the atomic composition of Co and Mn in $MnCo_2O_4$ is much closer to the stoichiometric ratio of preparation method rather than $CuCo_2O_4$ and $NiCo_2O_4$. It means there is oxygen deficiency in Elemental mapping analysis and corresponding EDX-mapping images of the $MnCo_2O_4$ spheres. It clearly elucidates homogeneous distribution of Mn, Co, and O elements further confirm the formation of pure $MnCo_2O_4$ materials.

The morphology and microstructures of the prepared catalysts were examined by SEM are shown in Figure 3.16. The morphology of all the catalysts are almost similar and very slight differences are observed in the particle size of all the samples. The presence of the Al and O in the catalysts did not greatly affect the morphology of the prepared samples and it is not very informative to explain the activity of the catalyst.

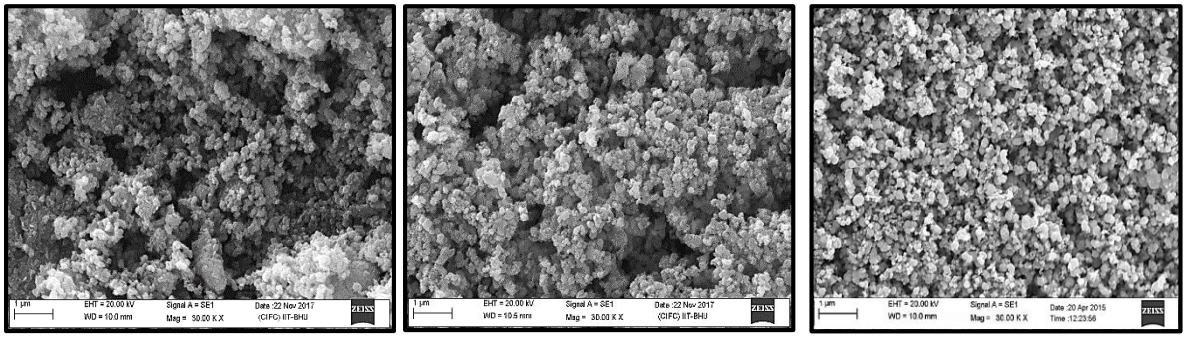

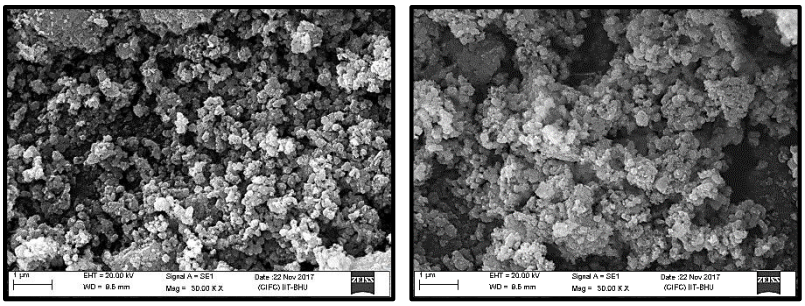

Figure 3.16. SEM micrographs of different metal loading (a) Cat-F, (b) Cat-G, (c) Cat-C_{RC} (d) Cat-H and (e) Cat-I

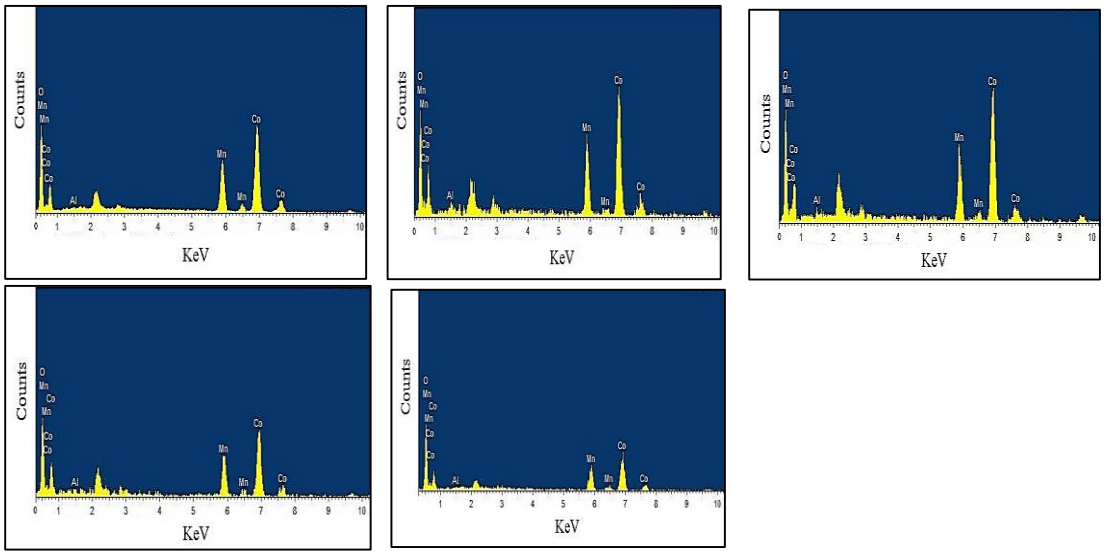

Figure 3.17. EDX spectra of different metal loading (a) Cat-F, (b) Cat-G, (c) Cat-C_{RC} (d) Cat-H and (e) Cat-I

The elemental composition of all the catalysts was determined by EDX as presented in Figure 3.16. It was evident from the results of the EDX analysis that all the samples were pure due to presence of Mn, Co, Al and O peaks only, there was no peak of other elements present in the spectra as shown in the figure. The presence of pure oxides phase from EDX was in good agreement with the XRD experiment results.

Table 3.2.7 displays the relative atomic abundance of ~~Mn, Co,~~ Al and O species present in surface layers of all the catalysts. It is very clear from the table that the ratio of atomic percentage of Mn and Co in all the catalysts were near to their stoichiometric amount (1:2) present in the catalyst. The EDX calculated atomic percent of the elements present in the catalysts was in good agreement with the XPS result. However, the atomic composition of oxygen was less than its theoretical values in all the catalysts.

Table 3.6. Weight % and atomic % (EDX elemental data) for Cat-F, Cat-G, Cat-H and Cat-I

	Cat-F		Cat-G		Cat-H		Cat-I	
Element	Weight %	Atomic %	Weight %	Atomic %	Weight %	Atomic %	Weight %	Atomic %
O K	20.34	48.03	27.85	58.12	32.60	58.62	32.60	58.62
Mn K	19.44	13.37	24.26	14.75	17.42	13.90	17.42	13.90
Co K	60.22	38.60	47.89	27.13	49.98	26.48	49.98	26.48
Total	100.00		100.00		100.00		100.00	

The lowest value of the oxygen was found in the Cat-I as compared to the others. Thus, the presence of surface defects or oxygen deficiencies in Cat-I catalyst, as compared to others, creates a high density of active sites to enhance the reaction performance of the catalyst in Table 3.6.

Effect of mono-metal (Rh) in binary spinel oxide, their morphology and microstructures of the prepared catalysts were examined by the SEM. The micrographs of Mn, Co, Al, Rh and O catalysts are shown in Figure 3.18. The micrographs of (a) Cat-J (b) Cat-K and (c) Cat-L were looking almost same and viewed the particles as an irregular shape or quasi-spherical. It was clearly seen from the figure that the particles of 0.2%Rh was smaller in size and homogeneously distributed as compare to others. While the nano-sphere like structure of the particles was observed in Cat-K was (Figure 3.18.b).

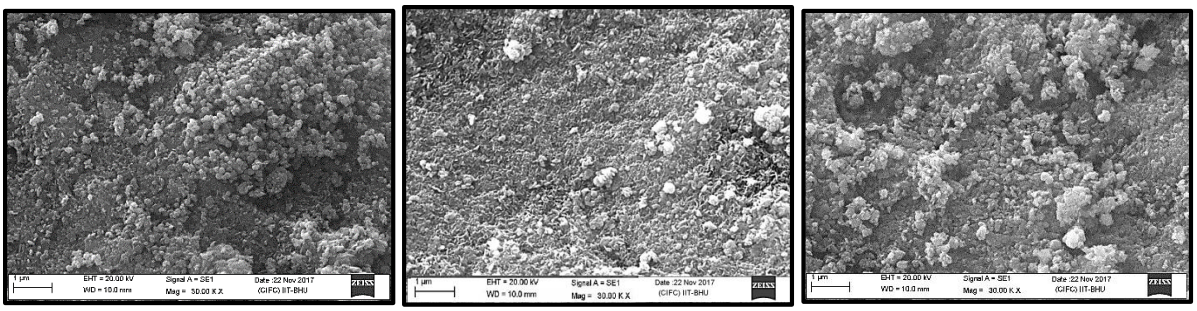

Figure 3.18. SEM images of (a) Cat-J, (b) Cat-K and (c) Cat-L.

The less agglomeration of the particles was found in Cat-L as compared to others. It was found that the particles of the catalysts were in nano-range. The particle sizes of the catalysts were in the range of 10–106 nm in the catalysts. The particles of the three catalysts were in the range of 82–120 nm, 63–82 and 58-97 nm respectively. The narrow particles size range of 51–78 nm was found in heterogeneous spinel catalyst. This particle sizes trend was the good agreement of crystallite sizes based on XRD peak width. However, the incorporation of Mn metal in the octahedral sites of normal Co_3O_4 spinel influences the crystallites, particle size as well as the morphology of the catalyst. The SEM results clearly show the difference in the morphology of the $MnCo_2O_4$ catalysts resulted by different promoter doping.

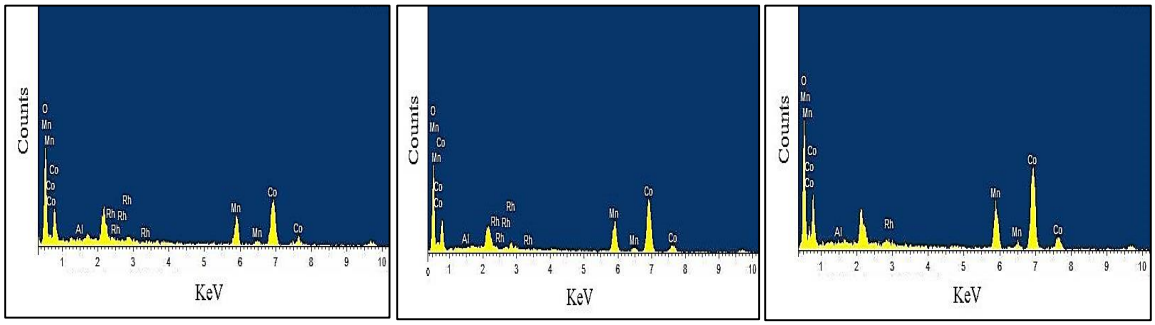

Figure 3.19. EDX spectra of catalyst (a) Cat-J, (b) Cat-K and (c) Cat-L.

Table 3.7. Atomic concentration of the catalysts attained by EDX

Element	Atomic%	Atomic%	Atomic%
O K	24.76	28.36	39.15
Co K	46.95	50.61	32.64
Mn K	16.29	12.33	17.41
Al K	11.63	7.97	9.87
Rh K	0.37	0.73	0.93
Total	100.00	100.00	100.00

EDX Measurement. EDX spectra of Cat-J, Cat-K and Cat-L catalysts are shown in Figure 3.19. The spectrum was obtained by the analysis of a single spot and also provided the information about the elemental composition of the catalysts. The presence of Mn, Co, Al, Rh and O elements in the catalysts was confirmed by the spectra. Table 3.7 summarizes the experimental ratio determined by EDX.

The experimental values of Mn and Co were not too much different from the theoretical values in the catalysts. It means that the Mn and Co in the catalysts are in the stoichiometric ratio. The experimental composition of oxygen in the catalysts deviated from the calculated theoretical values. The oxygen deficiencies in the catalysts create a high density of active center that are favorable to enhance the performance of the catalysts toward the reduction reaction.

The SEM micrographs (Figure 3.20.) show clearly large differences in the microstructure and morphology of the two Cat-K and V-W-Ti catalysts. The commercial catalyst show granular particles between 32 and 120 nm. As shown in SEM micrograph of Cat-K, the particles were comprised grains of course, fine and finest sizes than the rest and thus suitable for the better catalyst activity.

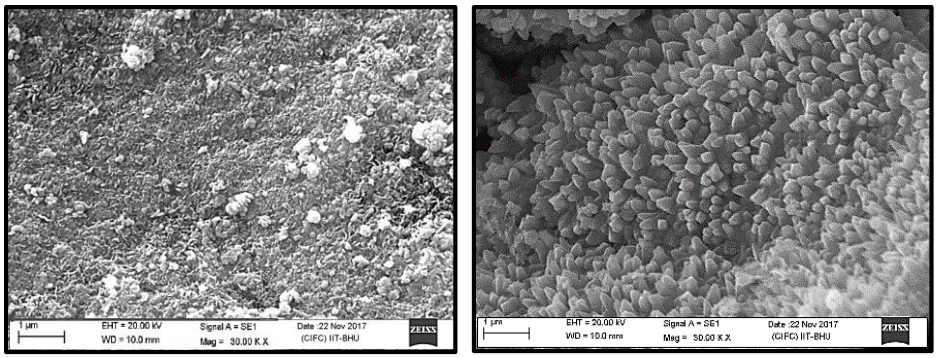

Figure 3.20. SEM images of (a) Cat-K and (b) V-W-Ti.

The SEM result is also in good agreement of XRD analysis. Particles of Cat-K are less agglomerated and heterogeneously distributed as compared to commercial catalyst. Thus, the preparation of the best catalyst in the present study considerably affect the particle size as well as morphology of the resulting catalysts.

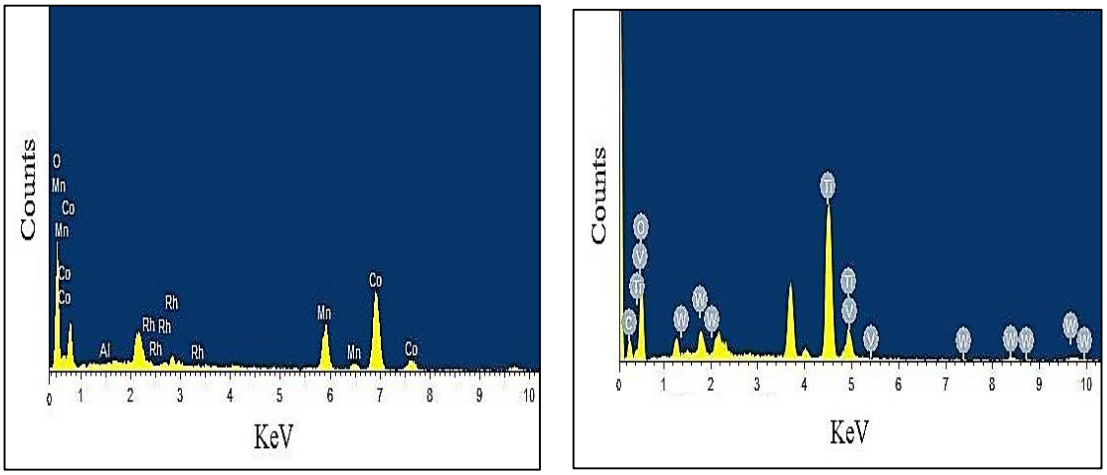

Figure 3.21. Energy dispersive x-ray spectra of catalyst (a) Cat-K and (b) V-W-Ti.

It was evident from the results of EDX analysis that Cat-K was pure due to the presence of Mn, Co, Al, Rh and O elements, there is no other element present in the spectra as shown in Figure 3.21. EDX results are also in good harmony of XRD results. However, the atomic composition of Co and Mn in Cat-K is much closer to stoichiometric ratio (0.97) of preparation

method. It means that there is oxygen deficiency present in Cat-K creating high density of active sites consequently enhancing the catalytic activity.

3.4. *FTIR results*

The main bands were located at 400-700 cm^{-1}, and were attributed to Mn species. FTIR transmission spectra of the catalysts are shown in Figure 3.22. The asymmetric stretching vibration at 1635.4 cm^{-1} is of the acrylates on Cat-K. Peak at 1528 cm^{-1} implies that in the initial stages of the SCR-NOx reaction the surface of $MnCo_2O_4$ catalyst is covered by acetates [41]. IR bands due to adsorbed NO_2, nitrite, and nitrate (NO_3) species were detected in the 1650-1000 cm^{-1} range. The bands centered at 1600 and 1200 cm^{-1} are attributed to the asymmetric and symmetric deformation of coordinated ammonia, respectively. The band at 1510 cm^{-1} is attributed to an amide ($-NH_2$) species in Cat-K [39].

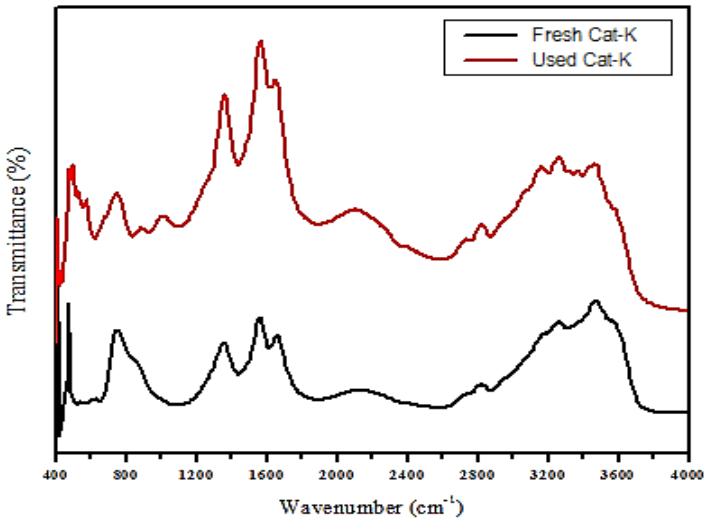

Figure 3.22. FTIR spectra of fresh and used Cat-K.

The bands at 1550 and 1570 cm^{-1} may be related to the intermediate of oxidation of ammonia. The band at 1300 cm^{-1} can be assigned to the symmetric deformation of ammonia co-ordinately bonded to one type of the Lewis acid sites [29].

3.5. BET results

The textural parameters such as the BET surface area, total pore volume, and average pore diameter of the catalysts are summarized in Table 3.8. It can be seen from the table that the surface area of $MnCo_2O_4$ (DCP) is the highest than the other catalysts. Typical isotherms of the different catalysts showing hysteresis loops of which desorption branch joined the adsorption curve around relative pressure 0.7. All the isotherms are type IV according to the IUPAC classification 1984, which suggests presence of mesoporous structure in the catalysts. The mesopores geometries of prepared catalysts exhibited H1 hysteresis loops. The order of surface area of the catalysts is as follows: Cat-C > Cat-B > Cat-A. The surface area of Cat-A and Cat-B is nearly identical, but the remarkable difference in the activity for the reduction of NO is observed and thoroughly discussed in the activity section. On the other hand, Cat-C has the smallest surface area than Cat-A and Cat-B, its performance is superior to Cat-A and Cat-B. The surprised observation of Cat-C may be due to structure sensitive reaction.

Table 3.8. Textural characterization of the prepared $MnCo_2O_4$ based on their preparation methods.

Catalyst	BET surface area ($m^2\ g^{-1}$)	Pore volume ($cm^3\ g^{-1}$)	Pore diameter (nm)
Cat-A	91.49	0.173377	68.465
Cat-B	83.596	0.110092	52.678
Cat-C	113.6519	0.177813	77.741

The specific surface area and pore size distribution were determined by BET and BJH methods with low temperature adsorption on three catalysts prepared by co-precipitation, nanocasting and reactive calcination methods. The BET surface area, pore volume and pore diameter of respective catalysts were tabulated in Table 4. S_{BET} = BET surface area. Total pore volume taken from the volume of N_2 adsorbed at $\sim P/P_0 = 0.99$. Average pore size calculated using desorption of N_2 adsorption isotherms by the Barrett− Joyner-Halenda (BJH) method.

Relatively high specific surface area (117.6 $m^2\ g^{-1}$) of the mesoporous $MnCo_2O_4$ catalyst for facilitating the NO reduction. It is evident from the tabulated data average particle size of Cat-R is highest as compared to Cat-F and Cat-S, which is below 1mm . Reactive calcined catalyst uniform distribution at low temperature show mesoporous (type IV with H1 type hysteresis loop). The average pore size for Cat- R is 4.174 nm higher than other two catalysts.

The BET surface area (117.6 $m^2\ g^{-1}$), pore volume and large hysteresis loop for catalyst Cat-R is more than 2.41 times than the catalyst prepared from convention method depends on calcinations strategy with increasing particle size trend as Cat-C_{RC}> Cat-C_{FA} > Cat-C_{SA}.

Table 3.9. BET Surface Area and Pore Parameters of Cat-C_{SA}, Cat-C_{FA} and Cat-C_{RC}

Catalyst	BET surface area ($m^2\ g^{-1}$)	Pore volume ($cm^3\ g^{-1}$)	Pore diameter (nm)
Cat-C_{SA}	48.79	0.043	3.529
Cat-C_{FA}	111.3	0.196	6.914
Cat-C_{RC}	117.6	0.139	4.174

The specific surface area and pore size distribution were determined by BET and BJH methods with low-temperature adsorption on the three catalysts prepared by the nano-casting method. The BET surface area, pore volume and pore diameter of respective catalysts. S_{BET} = BET

surface area. Total pore volume taken from the volume of N_2 adsorbed at $\sim P/P_0 = 0.99$. Average pore size calculated using desorption of the N_2 adsorption isotherms by the Barrett−Joyner−Halenda (BJH) method. The BET surface area, pore volume and pore diameter of all three catalysts are tabulated in Table 3.10.

Table 3.10. BET Surface Area, Pore volume and pore diameter of the cobaltite catalysts

Catalyst	BET surface area ($m^2\ g^{-1}$)	Pore volume ($cm^3\ g^{-1}$)	Pore diameter (nm)
$CuCo_2O_4$	79.019	0.093	4.716
$MnCo_2O_4$	111.3	0.196	6.914
$NiCo_2O_4$	61.916	0.079	4.099

Relatively high specific surface area (111.3 $m^2\ g^{-1}$) of the mesoporous $MnCo_2O_4$ catalyst for facilitating the NO reduction as given in Table 3.8. It is evident from the tabulated data BET surface area of the $MnCo_2O_4$ catalyst is the highest. $MnCo_2O_4$ catalyst showed mesoporous (type IV with H1 type hysteresis loop) uniform distribution at low temperature.

The BET surface area, pore volume and large hysteresis loop for the $MnCo_2O_4$ catalyst is more than 1.4 times the catalyst prepared by Cu and Ni precursors catalysts with the increasing particle size trend as $NiCo_2O_4 < CuCo_2O_4 < MnCo_2O_4$.

The textural properties of the metal cobaltite loading over γ-Al_2O_3 catalysts prepared by the RC route were determined by low temperature Nitrogen adsorption–desorption analysis. The isotherms of the catalysts were type IV according to De Boer classification. A hysteresis curve was observed at high relative pressure ranges for all the catalysts. The BET surface area of the optimum loading catalysts were higher than that of other catalysts, 113.65 m^2/g

for 30%$MnCo_2O_4/\gamma$-Al_2O_3 in comparison to rest all four. The surface areas for Cat-G, Cat-H and Cat I were comparable. The pore volume of Cat-F is 2 times than Cat G. Naturally, the textural properties of the Cat-C_{SA} was more favourable for the reaction than other catalysts. The most probable pore sizes for Cat-G and Cat-C_{SA} are 35.29 and 77.74 Å, respectively.

Table 3.11. Textural properties of all the catalysts prepared by RC

Catalyst	BET surface area ($m^2\ g^{-1}$)	Pore volume ($cm^3\ g^{-1}$)	Pore diameter (nm)
Cat-C_{RC}	113.6519	0.177813	7.7741
Cat-F	83.4387	0.089955	4.3124
Cat-G	47.6807	0.043046	3.529
Cat-H	48.7907	0.032647	4.3407
Cat-I	30.085	0.028218	4.8691

The textural properties of the catalysts were determined by nitrogen adsorption-desorption analysis. Typical adsorption-desorption isotherms for the Cat-J and its mono-metallic constituents (Cat-K and Cat-L) produced by RC. The nitrogen-sorption isotherms exhibited type IV isotherms with a separate H-1 hysteresis loop showing catalysts are mesoporous. The area of the hysteresis loop for catalyst Cat-K is negligible in comparison to other catalysts; this indicates the presence of open textured pores in the catalyst. The textural properties of the catalysts such as BET surface area, pore volume and average pore diameter is very clear from the table that Cat-L catalyst possessed the highest surface area of 101.29 m^2/g than the Cat-J (93.48 m^2/g) and Cat-L (99.31 m^2/g) catalysts. The porosity size distribution calculated from desorption data using BJH method, showed a narrow peak centered at 58nm indicating uniform mesopores of Cat-K, a lot smaller than macro-pore of Cat-J (74.98nm) and Cat-L (68.46nm). The BET surface-area measurement was in accordance with XRD studies that smaller the crystallite sizes as well as largest the surface area. These results indicate that the incorporation

of Rh to the supported Mn cobaltite increases both specific surface area and pore volume. Consequently, the features may be beneficial for reduction of NO.

Table 3.12. Textural Properties of the Prepared Catalysts

Catalyst	**BET surface area (m^2 g^{-1})**	**Pore volume (cm^3 g^{-1})**	**Pore diameter (nm)**
Cat-J	93.48	0.143	74.98
Cat-K	99.31	0.147	58.95
Cat-L	101.29	0.177	68.46

The specific surface area of the catalysts depends upon method of preparation. The surface area of the catalysts is mentioned in the Table 3.11. The mild acidic nature of γ-Al_2O_3 resulted Cat-K of larger surface area and comparable with V-W-Ti surface area.

Table 3.13. Crystallite size, particle size and surface area of the catalysts.

Catalyst	BET surface area (m^2 g^{-1})	Pore volume (cm^3 g^{-1})	Pore diameter (nm)
Cat-K	99.31	0.147	58.95
V-W-Ti	93.331	0.161	64.43

It can be evidenced from Table 3.13 that as the surface area of the catalysts increased the crystallite size as well as the particle size decreased. The nature of surface morphology and active site decides the catalyst performance in the reaction.

The various characterization outcomes conclude that Cat-K should perform the best in SCR of NOx based on the following observations:

The XRD results show that Cat-K exhibited the smallest crystallite size (7.97 nm) in comparison to other catalysts. The XPS and EDX results show that Cat-K possessed the highest oxygen vacancy in the lattice. The SEM micrograph depicts the smallest particle size of Cat-K. The BET surface area of Cat-K (99.31m^2/g) is comparable with commercial catalyst, V-W-Ti (93.331m^2/g).

The BET surface area of all the catalysts has been compiled in Table 3.14

Table 3.14. BET surface area of all the catalysts used in experiments

Catalyst	BET surface area (m^2/ g)
Cat-A	**91.49**
Cat-B	**83.60**
Cat-C_{SA}	**48.79**
Cat-C_{FA}	**111.3**
Cat-C_{RC}	**117.6**
Cat-D	**61.92**
Cat-E	**79.02**
Cat-F	**83.44**
Cat-G	**47.68**
Cat-H	**48.79**
Cat-I	**30.09**
Cat-J	**93.48**
Cat-K	**99.31**
Cat-L	**101.29**
Cat-K	**99.31**
V-W-Ti	**93.331**